# Experimental validation of the energy ship concept for far-offshore wind energy conversion

Aurélien Babarit, N. Abdul Ghani, E. Brouillette, S. Delvoye, M. Weber, A. Merrien, M. Michou, J.-C. Gilloteaux

Version of Record: https://www.sciencedirect.com/science/article/pii/S0029801821011872
Manuscript_562e2265955a2bb7ae938fe86bfb59e3

# Experimental validation of the energy ship concept for far-offshore wind energy conversion

A. Babarit[a]*[1], N. Abdul Ghani[a,b], E. Brouillette[a], S. Delvoye[a], M. Weber[a], A. Merrien[a], M. Michou[c], J-C. Gilloteaux[a]

[a] LHEEA, Ecole Centrale de Nantes - CNRS, Nantes, France

[b] Universiti Pertahanan Nasional Malaysia, Kuala Lumpur, Malaysia

[c] Watt&Sea, La Rochelle, France

* Corresponding author: aurelien.babarit@ec-nantes.fr

## Abstract

The energy ship is a new concept for offshore wind energy capture. It consists of a wind-propelled ship that generates electricity using water turbines attached underneath its hull. Since it is not grid-connected, the generated energy is stored aboard the ship (for instance, using batteries or through conversion to hydrogen using an electrolyzer).

This concept has received little attention until today. Particularly, there had not been yet an experimental proof-of-concept. In order to bridge this gap, an experimental platform has been developed at Centrale Nantes. It consists of a 5.5 m long catamaran equipped with a 240 mm diameter water turbine. The platform was tested in July 2019 on the river Erdre (France). Results show that a full-scale energy ship could deliver high levels of power production (megawatts); and that it is essential to optimize the water turbine induced drag in order to maximize energy production.

**Keywords:** offshore wind energy, energy ship, experiments

## 1. Introduction

[1] Now with Farwind Energy, 1 rue de la Noë, 44300 Nantes, France

With a global installed capacity over 35 GW [1] and the first floating wind farm having entered operation in 2017, the development of offshore wind has been a tremendous success. Nevertheless, with current technologies (bottom-fixed and floating wind turbines), offshore wind is limited to near-shore and relatively shallow water areas because grid-connection costs, installation costs and maintenance costs increase dramatically as the distance to shore and the water depth increase [2]. Therefore, the next frontier for offshore wind is to develop new technologies for far-offshore wind energy conversion.

In this respect, since 2017, the LHEEA lab. has been investigating the energy ship concept. This concept consists of a ship propelled by the wind (using sails) that generate electricity using water turbines attached underneath its hull. The electricity produced is stored on board, either in batteries [3] or in the form of fuel (hydrogen, ammonia, methanol, etc.[4] -[7]).

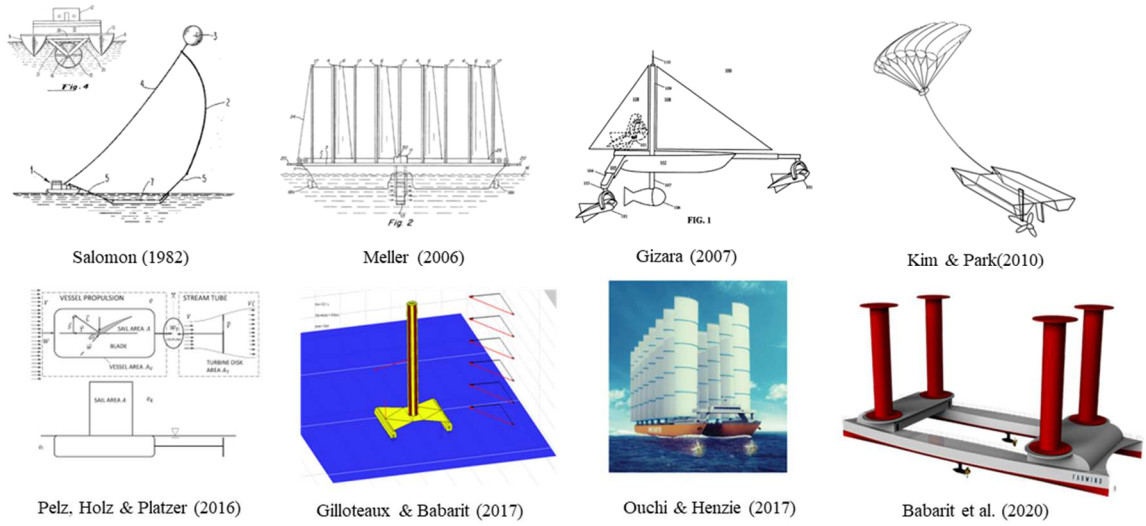


*Figure 1. Pictures of concepts of energy ships.*

Although the energy ship concept was patented in 1982 [4], it did not receive much attention until the end of the first decade of the 2000s. Thus, there has been only a limited number of energy ship proposals to date [4][8]-[13]. They are shown in Figure 1.

Regarding academic works, the energy ship has also been the focus of only few studies [3][5]-[7][10]-[16]. In 2009, Platzer and Sarigul-Klijn were the first to discuss the energy ship concept in a

scientific publication [14], proposing it as a way to increase hydrokinetic energy sources for water turbines. The following year, Kim and Park presented a concept that included kite sails flown at high altitude (1500 m) for wind propulsion, a catamaran for the hull, and hydrogen or methanol for the energy vector [5]. Using analytical and numerical modelling, they showed that an energy ship propelled by a 3,000 m² kite could generate approximately 1.2 MW if sailing in a wind of 20 knots. In[13], we showed that in the same wind conditions, an 80 m long catamaran equipped with four 30 m high rotor sails (Flettner rotors) and two 4 m diameter water turbines could generate 1.6 MW.

Furthermore, Pelz et al. [13]showed that a key parameter for maximizing energy recovery is the drag induced by the water turbine. This is because the power absorbed by the water turbine is equal to the product of the induced drag times the cube of the average flow velocity across the propeller disc, which is proportional to the ship velocity. If the induced drag is very large, then the ship velocity is very small, and the power absorbed tends towards zero. Conversely, if the drag is very small, the ship velocity tends towards that without the water turbine, but the power absorbed also tends towards zero. Between these two extremes, there is an optimum. We showed in [13] that this optimum can be significantly different from that for wind turbines or tidal turbines (because the input flow speed - the ship-velocity - depends on the induced drag).

The aim of the present study is two-fold. First, it aims to achieve an experimental proof-of-concept of the energy ship. Indeed, to our best knowledge, all studies carried out so far are desktop studies or based on numerical models. In this respect, we believe that it is of utmost importance to validate experimentally that significant amounts of energy can be produced with energy ships. Second, the aim is to investigate experimentally the effect of drag on energy production.

The remainder of the paper is organized as follows. The experimental platform is described in section 2. The tests and the experimental results are presented in section 3. Finally, in section 4, the energy performance of large-scale energy ships is extrapolated from the experimental data.

## 2 Description of the experimental platform

## 2.1 General arrangement

A second-hand Hobie Cat Tiger catamaran served as the base for the experimental platform (Figure 2). Her length is 5.51 m (18 feet). The rig consists of a 17 m² mainsail and a 4.15 m² jib. It has been designed to be handled by a crew of two people. This type of catamaran was selected for its low water resistance (which is essential to maximize energy production [10][13]), its low cost on the second-hand market, and because it fairly corresponds to a 1:14 scale version of the energy ship design described in [13].

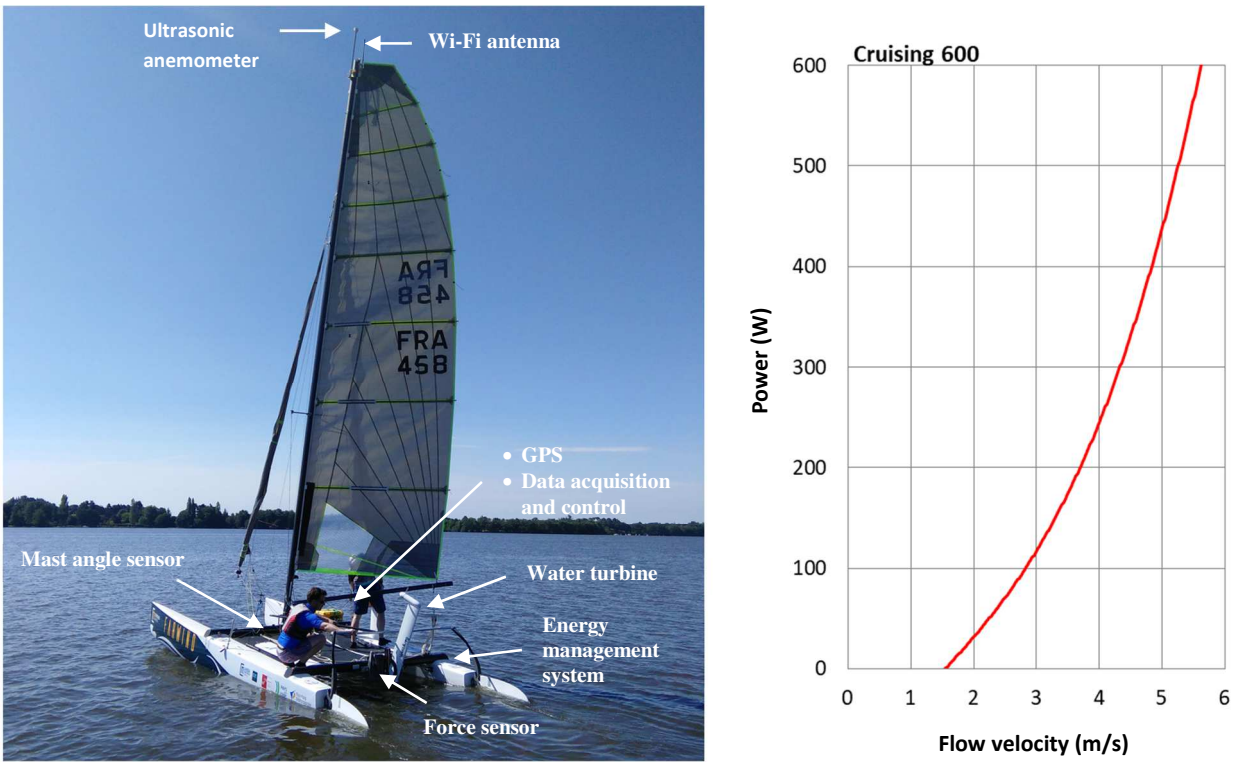


*Figure 2. Left: picture of the experimental platform. Right: performance of the Watt & Sea Cruising 600 water turbine*

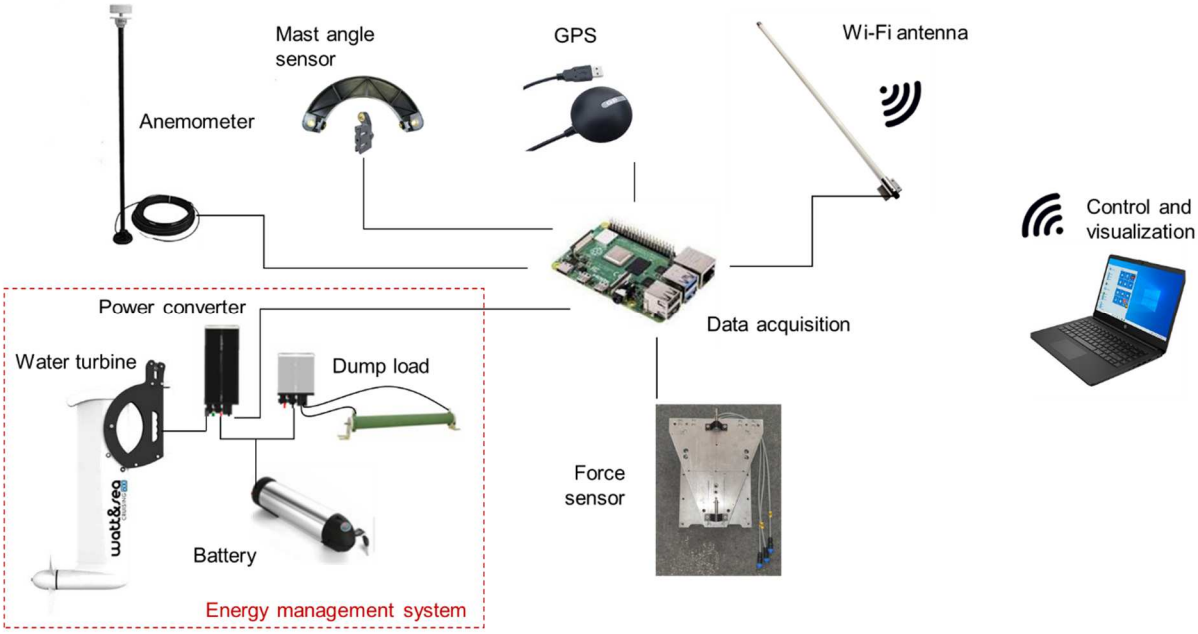


*Figure 3. Synoptic view of the instrumentation and equipment*

Figure 3 shows a synoptic view of the instrumentation and equipment which have been installed. A Watt & Sea Cruising 600 hydro-generator [19] was used for the water turbine. It has been mounted at the middle of the rear beam. The propeller diameter is 240 mm. According to the supplier, this configuration allows the production of 250 W of electrical power at a vessel speed of 4 m/s (Figure 2).

One of the objectives of the experimental campaign being to investigate the relationship between the drag induced by the water turbine and the energy production, a custom force sensor has been installed between the hydro-generator and the hull. The force sensor was designed and built at LHEEA (Figure 4). It consists of three HBM Z6 strain gauges mounted between two aluminum plates. Calibration results show that its accuracy is 0.4% of the maximal force (100 N).

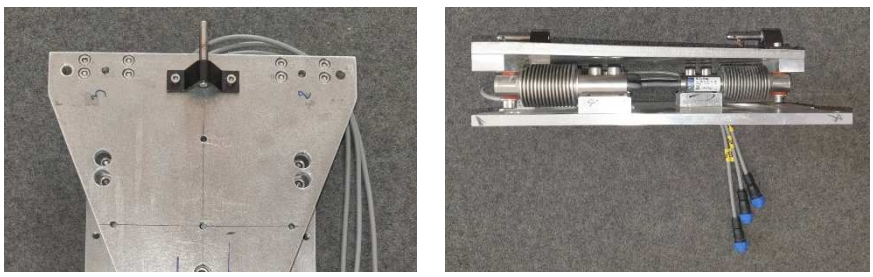

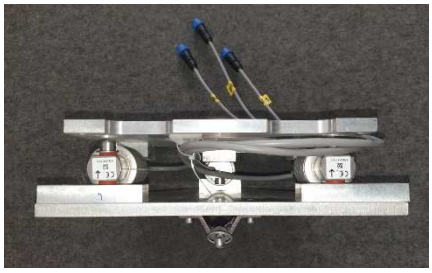

*Figure 4. Force sensor*

The energy management system has been integrated inside the starboard float. It includes a converter which controls the generator of the water turbine, a battery, and a discharge resistor (which was included to avoid overload in case of excess energy). The energy management system includes sensors to measure the energy production (voltage, current, power) and the rotational velocity of the water turbine. The resistive torque generated by the generator at the shaft of the propeller ($P_{shaft}$) is estimated from the measurement of the output current of the generator.

To measure the wind, a CV7-LCJ ultrasonic anemometer was installed at the top of the mast. As the Hobie Cat Tiger is equipped with a rotating wing mast, a mast angle sensor was positioned at the bottom of the mast in order to be able to correct the wind angle measurement.

The control and data acquisition system is based on a Raspberry Pi 3. It is integrated in a waterproof case (Pelicase) on the starboard float deck. It is connected to the various sensors by wire links. The acquisition software was developed at LHEEA in Python. It allows the continuous recording and storage of the measured data in an ASCII file in a memory card on board the platform, as well as the broadcast of the data through Wi-Fi (a Wi-Fi antenna was installed at the top of the mast). This feature allowed the experiments to be monitored and controlled in real-time by a team which stayed on the riverbank. In particular, the output voltage of the generator of the water turbine (and therefore the drag, see following section) was controlled remotely, which allowed the crew on board the catamaran to focus on navigation.

## 2.2 Water turbine calibration

The generator output voltage of the water turbine is controlled by the converter of the energy management system. This allows controlling the generator current and therefore the resistive torque on the shaft of the propeller, thus the propeller rotational velocity, thus the induced drag and energy production.

By default, the controller of the converter automatically optimizes the generator output voltage in order to extract the maximum power from the water turbine. For the experiments, it was modified in order to enable a given value of the generator output voltage to be prescribed (and thus the water turbine drag force).

To determine the characteristics of the water turbine (drag force and generated power as function of the generator setting and flow velocity), experiments were carried out in the towing tank of Ecole Centrale de Nantes. The experimental setup is shown in Figure 5. The water turbine and its force sensor were mounted on the carriage. The propeller shaft was submerged 520 mm deep. Tests were carried out for a range of carriage velocities of 1.5 - 6.0 m/s. The generator output voltage was varied in the range 10 to 50 V. The drag force was measured using the same sensor as that used for the experimental platform (Figure 4).

*Figure 5. Experimental set-up for the characterization of the water turbine*

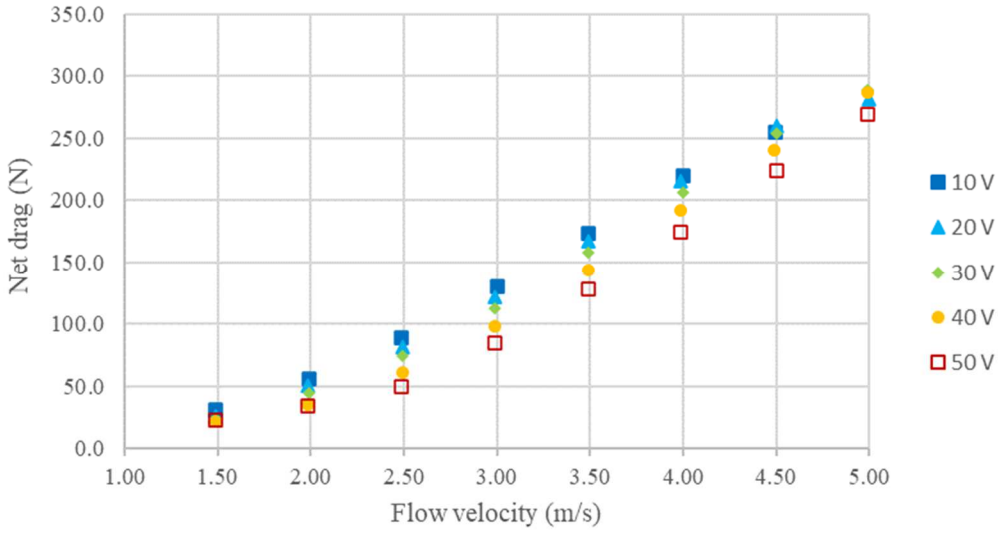


*Figure 6. Water turbine's net drag force as function of the flow velocity and generator output voltage.*

Figure 6 shows the measured water turbine net drag force as function of the flow velocity and generator output voltage. The net drag force is the measured drag force minus the measured drag force without the propeller. One can see that, as expected, the drag force decreases with increasing output voltage. However, the controllability of the drag force appears to be limited as, for a given flow velocity, the minimum drag force (which is obtained for an output voltage of 50 V) is at least 56% of the maximum drag force (obtained for output voltage 10 V).

## 3 Experiments

Tests were carried out on July 2nd, 2019 at Plaine de Mazerolles on the Erdre river (France). At this location, the river is wide, and the current is negligible. The wind conditions were light (1 to 7 m/s).

### 3.1 Method

The experimental method consisted of a series of roundtrips on beam reach (see example in Figure 7). This wind direction was chosen because it corresponds to the point of sail for which the performance of energy ship is maximum[13]. On each round trip, the control setting (generator

output voltage) was changed in order to study its effect on energy production. Eventually, four usable data records were obtained (labelled Run02, Run03, Run04, Run05, See Figure 7). Of these four recordings, a total of seventeen crossings of the river were made.

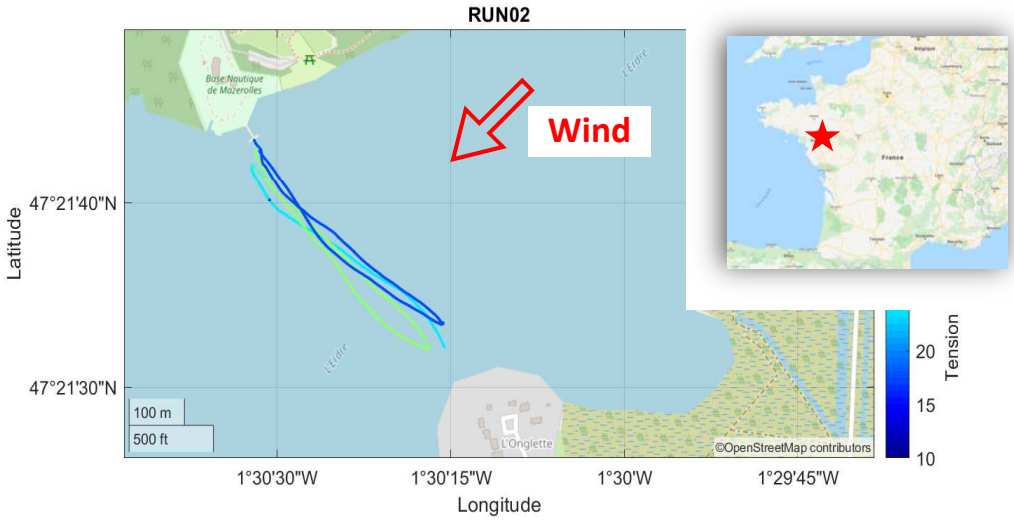


*Figure 7. Example of GPS trajectories during the experiments. The colors indicate the setting (output voltage) of the generator of the water turbine. Background picture and map: OpenStreetMap*

## 3.2 Data processing

Figure 9 shows the time recording of some of the data collected during Run02 (true wind speed, boat velocity, generator output voltage, true wind angle). One can see that there are significant oscillations. They are related on the one hand to the inability of the crew to perfectly maintain heading, but also and above all also to significant variations in the wind (both in strength and direction) over the test area (inland waters).

The seventeen river crossings were analyzed one by one in order to identify measurement intervals during which the experimental signals were stable (shaded areas in Figure 9). The signals were then averaged over each of these intervals. Standard deviations were also calculated in order to keep trace of the data quality.

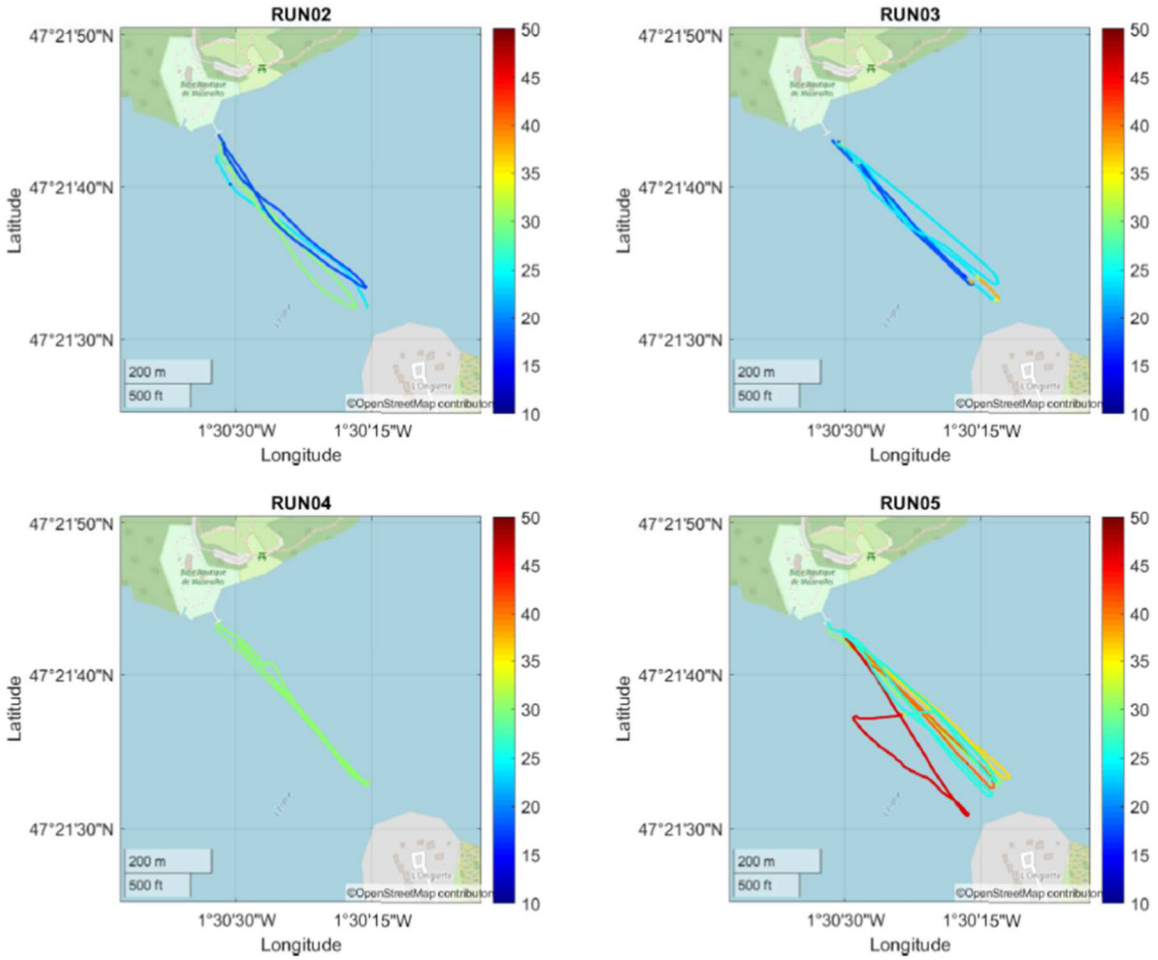


158 *Figure 8. GPS traces of the experiments. The colors indicate the setting (output voltage) of the*

159 *generator of the water turbine. Background picture: OpenStreetMap*

160 Based on the processed data, the water turbine drag coefficient $C_T$ and the energy ship power

161 coefficient $C_P$ were calculated. For the water turbine drag coefficient, we used the usual definition:

162 $$C_T = \frac{D_{net}}{\frac{1}{2}\rho_{water} A_{WT} SOG^2}$$

163 (1)

164 where $D_{net}$ is the net water turbine drag force (measured drag force minus drag force on the water

165 turbine mast), $A_{WT}$ is the water turbine disc surface area, and $SOG$ is the boat velocity.

166 For the power coefficient $C_P$, the usual definition for a water turbine is:

$$C_P = \frac{P_{shaft}}{\frac{1}{2}\rho_{water} A_{WT} SOG^3} \quad (2)$$

where $P_{shaft}$ is the mechanical power at the shaft of the water turbine generator.

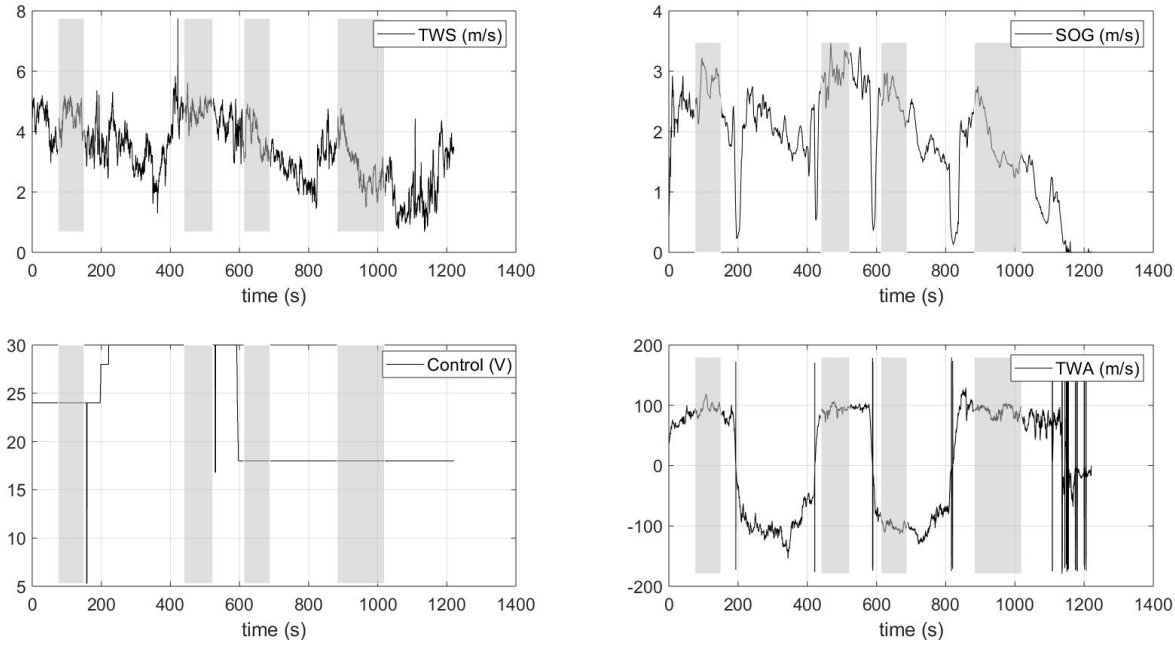


*Figure 9. Example of raw data measured Run02. Top left panel: true wind speed. Top right panel: boat speed. Bottom left: generator output voltage. Borrom right: true wind angle. The shaded areas correspond to the time windows which were retained for analysis.*

However, we think that this definition is not appropriate for the energy ship because it is not based on the actual energy source (which is the wind). Therefore, for an energy ship, we instead propose to define the power coefficient as:

$$\tilde{C}_P = \frac{P_{shaft}}{\frac{1}{2}\rho_{air} A_S TWS^3} \quad (3)$$

where $A_s$ is the sail area (21.15 m² in the experiments).

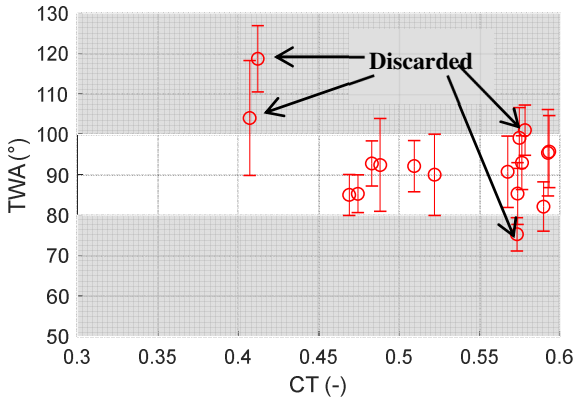


*Figure 10. Illustration of the data obtained after analysis. The figure shows the average true wind angle as function of the water turbine drag coefficient.*

Figure 10 shows an example of the data obtained after processing. One can see that despite the crew's best effort to keep the true wind angle close to 90 degrees during the experiments, there are data points that deviate significantly from this objective. Since the true wind angle is a key driver of energy ships' velocity and energy performance[13], and since the aim of the paper is to investigate the effect of the water turbine's drag force on performance, only the data for which the average true wind angle is between 80 ° and 100 ° is retained in what follows.

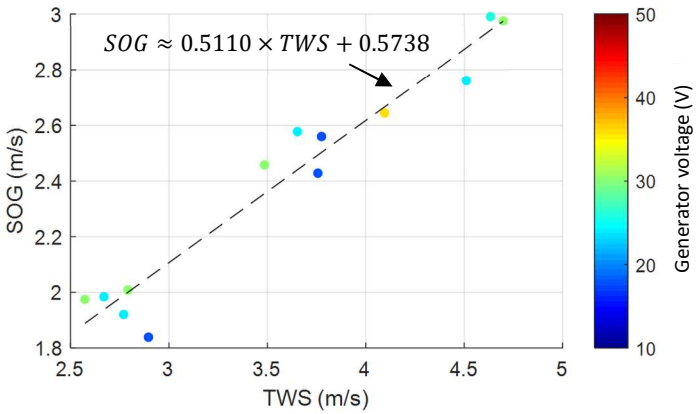


*Figure 11. Boat velocity (SOG) as function of the true wind speed (TWS) and generator output voltage. The water turbine was in operation.*

Figure 11 shows the average boat velocity as function of the average true wind speed and the generator output voltage. The range of average wind speed is 2.5 - 5.0 m/s. It appears that, when the water turbine is in operation, the boat speed is approximately equal to half the true wind speed. Unfortunately, no recording of the boat speed without the water turbine was made. Nevertheless, it is typical for a sport boat (such as the catamaran used in the experiments) sailing at a 90 degrees true wind angle that its speed is in the order of the true wind speed (if not exceeding).

### 3.3 Results

Table 1 summarizes the results of the data processing. The data for each row corresponds to the average of the raw data over the intervals selected for analysis (see Figure 9).

Figure 12 shows the drag coefficient and power coefficient as function of the output voltage. In the left panel, one can see that the drag coefficient decreases with increasing voltage (as observed in the towing tank experiments). Note also that the range of variation of the drag coefficient is relatively limited as it drops by only 20% when the output voltage goes from 18 to 36 V. If the full range of variation of the voltage had been used (10 to 50V), the drag coefficient could have varied by about 40%

| Crossing | Run number | TWS (m/s) | TWA (°) | SOG (m/s) | Output voltage (V) | $C_T$ | $\tilde{C}_P$ |
|---|---|---|---|---|---|---|---|
| 1 | 3 | 3.77 (0.20) | 82.2 (6.1) | 2.56 (0.14) | 18 | 0.590 (0.034) | 0.133 (0.026) |
| 2 | 4 | 2.57 (0.43) | 85.0 (5.1) | 1.97 (0.21) | 30 | 0.469 (0.053) | 0.263 (0.097) |
| 3 | 4 | 2.79 (0.48) | 85.3 (4.7) | 2.01 (0.14) | 30 | 0.474 (0.057) | 0.230 (0.083) |
| 4 | 3 | 3.65 (0.63) | 85.4 (7.6) | 2.58 (0.29) | 24 | 0.573 (0.058) | 0.214 (0.080) |
| 5 | 3 | 2.77 (0.63) | 90.0 (10.0) | 1.92 (0.27) | 24 | 0.522 (0.050) | 0.219 (0.139) |
| 6 | 2 | 2.90 (0.74) | 90.8 (8.9) | 1.84 (0.44) | 18 | 0.567 (0.071) | 0.138 (0.495) |
| 7 | 5 | 4.10 (0.29) | 92.2 (6.4) | 2.64 (0.23) | 36 | 0.509 (0.052) | 0.189 (0.046) |
| 8 | 3 | 2.67 (0.53) | 92.5 (11.5) | 1.98 (0.37) | 24 | 0.488 (0.056) | 0.217 (0.097) |
| 9 | 5 | 3.49 (0.25) | 92.8 (5.6) | 2.46 (0.15) | 30 | 0.483 (0.044) | 0.217 (0.044) |
| 10 | 2 | 4.70 | 93.0 (6.7) | 2.98 | 30 | 0.576 | 0.180 |

| | | | | | | | |
|---|---|---|---|---|---|---|---|
| | | (0.59) | | (0.22) | | (0.051) | (0.044) |
| 11 | 5 | 4.63 (0.95) | 95.5 (10.7) | 2.99 (0.47) | 26 | 0.592 (0.045) | 0.174 (0.048) |
| 12 | 2 | 4.51 (0.43) | 95.8 (8.9) | 2.76 (0.28) | 24 | 0.593 (0.045) | 0.137 (0.036) |
| 13 | 3 | 3.76 (0.64) | 99.1 (7.5) | 2.43 (0.35) | 18 | 0.575 (0.048) | 0.116 (0.032) |

*Table 1. Experimental results. The numbers between parenthesis are the standard deviations.*

In the right panel, one can see that, as expected, varying the output voltage - and therefore the drag - influences energy production. For the range of tested voltage, the power output appears to increase with increasing voltage (and thus decreasing water turbine drag). Unfortunately, the experimental results do not allow to determine what is the optimal drag value (since the maximum production is obtained for the upper bound of the test interval). Further testing with higher voltage would be necessary.

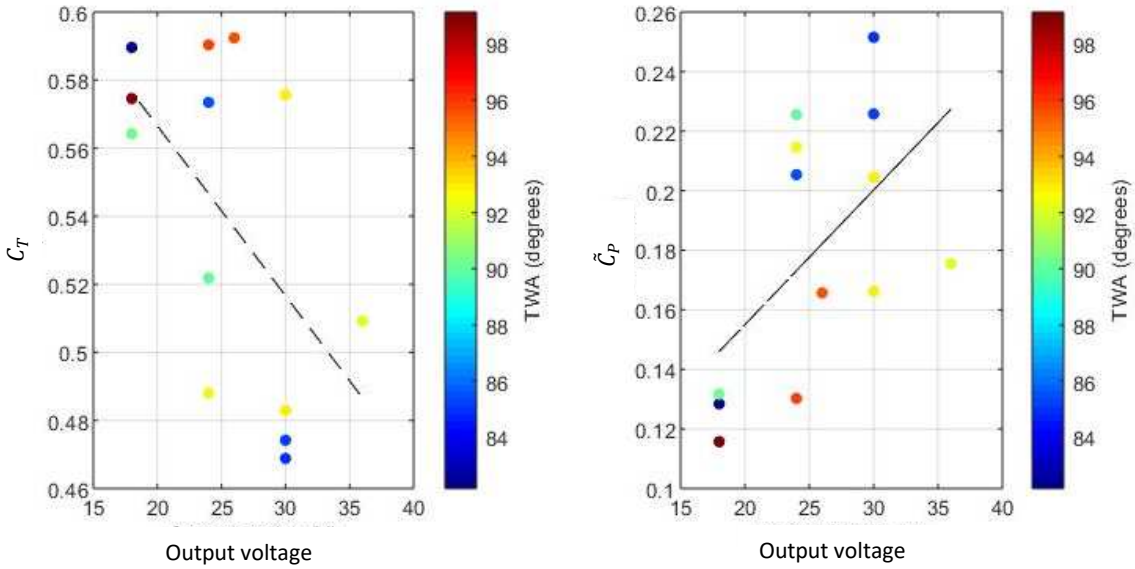


*Figure 12. Drag and power coefficient of the water turbine as function of the generator output voltage and true wind angle (TWA).*

## 4 Energy performance of a large-scale energy ship

### 4.1 Estimate based on the experimental data.

Based on the experimental results, let us estimate the energy performance of a large-scale energy ship. It is assumed that the scale of the experiments is 1:14, as for this scale the length of the 1:1 ship would be 77 m which is close to that of the energy ship design shown in Figure 1 (80 m). It is further assumed that the design of the water turbine of the large-scale energy ship has the same hydrodynamic characteristics (drag coefficients, power coefficients) as that of the water turbine used in the experiments. Finally, the estimate is based on the data of crossing #3 in Table 1 despite crossing #2 has the best power coefficient $\tilde{C}_P$, because the latter looks like an outlier.

| | | **Experiments (1:14 scale)** | **1:1 scale** |
|---|---|---|---|
| **Length** | *m* | 5.51 | 77 |
| **Sail area** | *m²* | 21.15 | 4 145 |
| **Displacement (estimate)** | *kg* | 350 | 960 000 |
| **Wetted surface area (estimate)** | *m²* | 4.7 | 921 |
| **Water turbine diameter** | *m* | 0.24 | 3.36 |
| $C_T$ | - | 0.474 (0.057) | 0.474 (0.057) |
| $\tilde{C}_P$ | - | 0.230 (0.083) | 0.230 (0.083) |
| $TWS_{10}$ | *m/s* | 2.79 (0.48) | 7.21 (1.25) |
| **TWA** | ° | 85.3 (4.7) | 85.3 (4.7) |
| **SOG** | *m/s* | 2.01 (0.14) | 7.5 (0.5) |
| **Froude number** | - | 0.27 | 0.27 |
| **Reynolds number** | - | 1.1E+07 | 5.8E+08 |
| **Shaft power without correction (Reynolds)** | *kW* | **0.063 (0.032)** | 650 (330) |
| **Shaft power with correction (Reynolds)** | *kW* | N/A | **830 (450)** |

*Table 2. Estimate of the energy production of a full-scale energy ship based on the experimental results.*

The estimates are presented in Table 2. The data for the 1:1 scale were obtained using Froude-scaling except for the true wind speed at 10 m altitude ($TWS_{10}$), and for the energy production. Indeed, for the true wind speed, the direct application would give the true wind speed at 140 m

altitude. Because of the Earth atmospheric boundary layer, the actual value at 10 m altitude is significantly smaller. In the present study, it is estimated using the classical power law:

$$TWS(z) = TWS_{10}\left(\frac{z}{10}\right)^{0.14} \quad (4)$$

where *z* is the altitude.

For the energy production (mechanical power on the shaft), two values were calculated: one without considering that the Reynolds numbers are different between scale 1:14 and scale 1:1, and the other taking it into account. The first case corresponds to the direct application of the Froude scale. In the second case, a correction is applied to consider the effect of scale distortion. Indeed, at the 1:14 scale, the drag force of the hull can be written:

$$R_{W,1:14} = \frac{1}{2}\rho_{water} A_{W,1:14} C_{W,1:14} {U_{1:14}}^2 \quad (5)$$

where $A_{W,1:14}$ is the wetted surface of the hull, $C_{W,1:14}$ is the hull resistance coefficient, and $U_{1:14}$ is the ship velocity. As the forward speed was moderate in the tests ($F_n \sim 0.27$) and since the hull consists of two thin floats, the component of the hull resistance coefficient associated with wave resistance is neglected. Thus, the hull resistance coefficient reduces to its friction component $C_{f,1:14}$. According to ITTC [18], it can be written:

$$C_f = \frac{0.075}{(\log_{10} \mathrm{Re} - 2)^2} \quad (6)$$

The application of the ITTC formula shows that the friction coefficient is of the order of 0.0029 at scale 1:14, whereas it is 0.0016 at scale 1:1. Therefore, the direct application of Froude scaling overestimates the full-scale hull resistance by up to 80%.

Let us then estimate energy production considering this effect. Let us denote $\Delta R_W$ the difference in hull resistance between that obtained using Froude scaling and that estimated considering the full-scale Reynolds number:

$$\Delta R_W = 14^3 R_{W1:14} - \frac{1}{2}\rho S_{W,1:1} C_{W,1:1} {U_{1:1}}^2$$

$$\Delta R_W = 14^3 \left( R_{W1:14} - \frac{1}{2}\rho S_{W,1:14} C_{W,1:1} {U_{1:14}}^2 \right)$$

(7)

To estimate the additional power available to the water turbine, let us consider the equation of motion of the ship at equilibrium:

$$T = R_W + D$$

(8)

Where $T$ is the thrust delivered by the sails and $D$ is the water turbine drag force. Equation 8 can be rewritten:

$$D = T - R_W$$

(9)

In particular, at the 1:14 scale:

$$D_{1:14} = T_{1:14} - R_{W1:14}$$

(10)

And at scale 1:1:

$$D_{1:1} = T_{1:1} - R_{W1:1}$$

(11)

For the thrust delivered by the sails, the Reynolds number at the 1:14 scale is of the order of $10^5$ against $10^6$ for scale 1:1. Thus, the air flow is fully turbulent, and we can therefore assume that there is no of effect of scale. Therefore:

$$D_{1:1} = 14^3 T_{1:14} - R_{W1:1} \quad (12)$$

By injecting Equation 10 into Equation 12:

$$D_{1:1} = 14^3 (D_{1:14} + R_{W1:14}) - R_{W1:1} \quad (13)$$

Finally:

$$D_{1:1} = 14^3 \left( D_{1:14} + \frac{1}{2} \rho S_{W,1:14} C_{f,1:14} {U_{1:14}}^2 \right) - \frac{1}{2} \rho S_{W,1:1} C_{f,1:1} {U_{1:1}}^2$$

$$D_{1:1} = 14^3 \times \frac{1}{2} \rho \left( \frac{\pi}{4} {D_{1:14}}^2 C_T + S_{W,1:14} \left( C_{f,1:14} - C_{f,1:1} \right) \right) {U_{1:14}}^2 \quad (14)$$

The numerical application of this latter equation shows that the drag induced by the water turbine must be increased by 28% for the speed of the ship at scale 1:1 to correspond to that of the ship at scale 1:14. The power production being proportional to the water turbine drag, it is also increased by 28%. Thus, by a wind of force 4 (7.2 m/s) on the Beaufort scale, the 1:1 scale energy ship may therefore be capable of producing over 800 kW.

### 4.2 Estimate based on a numerical model validated against the present experiments.

Another approach to estimate the energy performance of a large-scale energy ship is to use a numerical model. In such approach, the experimental results are used to validate the model. Then, the model can be used to determine the velocity and power performance at large scale.

In the present study, the numerical model is based on that presented in[13]. That model requires as inputs the characteristics of the rig (dimensions, aerodynamic coefficients), of the hull (dimensions and residuary coefficients) and of the water turbine. They are described in what follows.

As mentioned previously, the rig of the Hobie Cat Tiger consists of a mainsail (17 m²) and a jib (4.15 m²). Unfortunately, to our knowledge, the aerodynamic coefficients for this exact configuration

are not available in the literature. Therefore, we used as an approximation the aerodynamic coefficients of a mainsail of aspect ratio 6 (Figure 13).

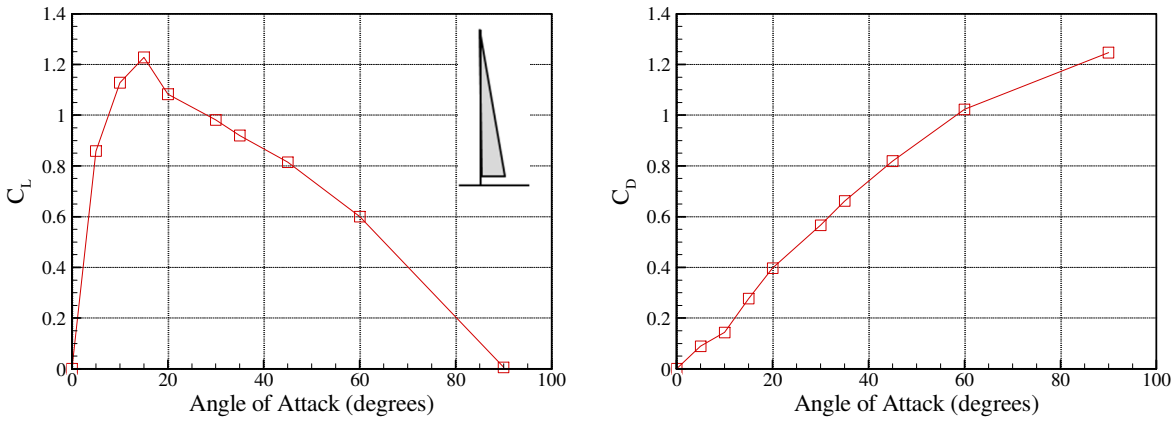


*Figure 13. Lift (left) and drag (right) coefficients of a Bermudan sail of aspect ratio 6. Source: Figure 127 in [20]*

The hull was 3D-scanned in order to achieve a digital-twin. Her estimated displacement during the experiments is 350 kg (light ship: 180 kg, crew: 150 kg, force sensor: 6kg, water turbine: 9 kg, other sensors and equipment: 5 kg). For that displacement, the hull wetted surface is 4.7 m². The hull residuary resistance coefficients were obtained using the REVA software [21] (Figure 14).

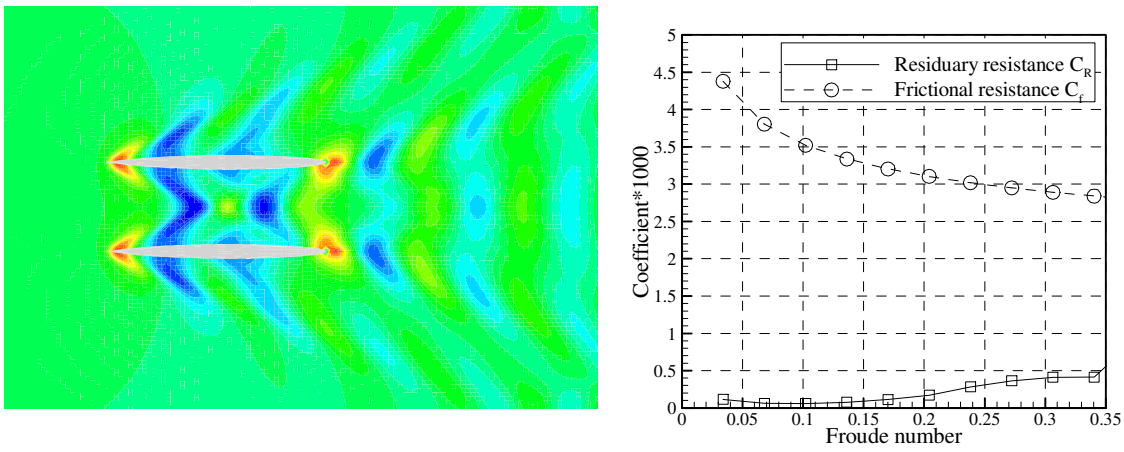


*Figure 14. Left: Picture of the wave field for ship velocity 2 m/s (Froude number 0.272). Right: hydrodynamic coefficients.*

To accurately estimate the water resistance, it is also important to take into account the appendages. In this respect, the Hobie Cat Tiger is equipped with two daggerboards (0.42 m²) and two rudders (0.27 m²). They were modelled as NACA 0009 profile.

For the water turbine coefficients, the results obtained in the towing tank experiments were used (see section 2.2).

Table 3 shows the comparison of the experimental results and of the numerical model for wind conditions corresponding to crossing #3 ($TWS_{10} = 10$ m/s, TWA = 85.3°). The velocity predicted by the numerical model is 2.12 m/s, which is 5% greater than in the experiments (while falling in the uncertainty range). The predicted power is 57 W, thus 10% smaller than in the experiments. Therefore, the agreement between the numerical model and the experiments is very good.

| | | **1 :14 scale** | | **1 :1 scale** | |
|---|---|---|---|---|---|
| | | **Experiments** | **Numerical model** | **Scaled water turbine** | **Optimized water turbines** |
| **Length** | *m* | 5.51 | 5.5 | 77 | 77 |
| **Sail area** | *m²* | 21.15 | 21.15 | 4 145 | 4 145 |
| **Displacement** | *kg* | 350 (estimate) | 350 | 960 000 | 960 000 |
| **Wetted surface area** | *m²* | 4.7 (estimate) | 4.7 | 921 | 921 |
| **Water turbine diameter** | *m* | 0.24 | 0.24 | 3.36 | 4. |
| $C_T$ | - | 0.474 (0.057) | 0.508 | 0.508 | 0.274 |
| $TWS_{10}$ | *m/s* | 2.79 (0.48) | 2.79 | 10. | 10. |
| **TWA** | ° | 85.3 (4.7) | 85.3 | 90 | 90 |
| **SOG** | *m/s* | 2.01 (0.14) | 2.12 | 8.53 | 9.61 |
| **Froude number** | - | 0.27 | 0.29 | 0.31 | 0.35 |
| **Reynolds number** | - | 1.1E+07 | 1.2E+07 | 6.7E+08 | 7.4E+08 |
| **Shaft power** | *kW* | 0.063 (0.032) | 0.057 | 1 460 | 2 320 |

*Table 3. Comparison of the experimental results and the numerical results at 1:14 scale, and estimates of power production of a large-scale energy ship with the scaled water turbine and optimized water turbines.*

Table 3 also shows velocity and power performance results for the large-scale energy ship. Note that for the large-scale ship, it is assumed that the sail area is distributed over two masts of height 90 m each. This is because the total sail area of the 1:1 ship is 4 145 m², which is 73% more than the world greatest Bermudan rig (2 385 m², [22]). Thus, 45 m has been used for the reference altitude for the calculation of the wind speed in Equation 4 (instead of 63 m for the direct application of the Froude-scale).

Two versions of the large-scale scale energy ship were considered. In the first one (scaled water turbine), it is assumed that the ship is equipped with a water turbine whose hydrodynamic coefficients are the same as in the experiments (as in the previous section). According to the model, that ship would sail at a velocity of 8.53 m/s (16.5 knots) and it could deliver 1 460 kW of mechanical power on the shaft of the generator for a true wind speed of 10 m/s at 10 m altitude and a true wind angle of 90 degrees.

In the second version, it is assumed that the ship is equipped with two water turbines of 4 m diameter, and that the design of the rotor of the turbines is optimized. Indeed, it was shown in Pelz et al. [10]that a key parameter for maximizing energy recovery is the drag induced by the water turbine, and that the optimal drag can be significantly different from that for wind turbines or tidal turbines[13]. Therefore, in the present study, it is assumed that the water turbine's rotor is such that it can deliver the same thrust and power as an actuator disc with 80% efficiency, and the induction factor is optimized in order to maximize power. Results show that that ship could produce 2 320 kW for a true wind speed of 10 m/s and a true wind angle of 90°. Thus, despite sailing slower than the ship with the scaled water turbine, it would produce 37% more power. This can be explained by the significantly smaller induction factor of the turbines' rotors which minimizes the hydrodynamic losses (see section 2.2 in[13]).

Finally, in agreement with[13], it appears that power production of order of a few megawatts is feasible for large-scale energy ships for wind conditions of force 5 on the Beaufort scale, wind conditions which are very common in the high seas.

## 5 Conclusion

In this paper, we presented an experimental proof-of-concept of the energy ship concept. It is based on a 5.5 m long sailing catamaran equipped with a 600 W hydro-generator. A power production (mechanical power) of 63 W was measured in the experiments for a true wind speed of 2.79 m/s and a true wind angle of 85.3°. It corresponds to approximately 2 MW for a wind of force 5 on the Beaufort scale for a large-scale energy ship. Thus, the experiments confirm that the energy ship concept can lead to power production levels comparable to wind turbines.

The experimental results also confirm the importance of optimizing the water turbine drag to maximize power production. However, unfortunately, it was not possible to determine the optimum drag in the experiments as it is out of the range achievable by the used water turbine. This issue may be addressed in future work. Note that it may require the development of new water turbine rotor designs dedicated to energy ships as their optimal induction factor may be significantly different from that of wind turbines or tidal turbines. Such turbine design studies have already been started by Siddappaji and Turner [23]. Also, it will be important to reduce the ship drag to a bare minimum and to optimize the sail aerodynamics, which may be achieved by switching to hydrofoil boats, as proposed by Platzer and Sarigul-Klijn [24]. Furthermore, it will be crucial to optimize the technical and economic aspects by using autonomously operating energy ships. In this respect, the techno-economic optimization studies already performed by Pelz et al. [10]for displacement boats may be extended to hydrofoil boats.

## Acknowledgements

This work was supported by the Pays de la Loire Region, France; and Nantes Métropole, Nantes, France [WEAMEC project WEREVER_DEMO].

## References


[1] J. Lee, P. Zhao (2021) GWEC Global wind report 2021, Global Wind Energy Council

[2] Offshore wind programme board, Transmission costs for offshore wind - final report, April 2016

[3] M.F. Platzer and N. Sarigul-Klijn (2015) Energy ships and plug-in electric vehicles: are they the key for a rapid transition to an emission-free economy?, in Proc. Of the ASME 2015 International Mechanical Engineering Congress and Exposition (IMECE), Houston, Texas, USA.

[4] R.E. Salomon (1982) Process of converting wind energy to elemental hydrogen and apparatus therefore. U.S. Patent 4335093A

[5] J. Kim, C. Park (2010) Wind power generation with a parawing on ships, a proposal. Energy, Vol. 35, pp. 1425-1432

[6] A. Babarit, J-C. Gilloteaux, G. Clodic, M. Duchet, A. Simoneau, M.F. Platzer (2018) Techno-economic feasibility of fleets of far offshore hydrogen-producing wind energy converters. International Journal of Hydrogen Energy, Vol. 43(15), pp. 7266-7289

[7] A. Babarit, J-C. Gilloteaux, E. Body, J-F. Hétet (2019) Energy and economic performance of the FARWIND energy system for sustainable fuel production from the far-offshore wind energy resource. In Proc. Of the 14th International Conference on Ecological Vehicles and Renewable Energies (EVER), Monaco

[8] M. Meller (2006) Wind-power linear motion hydrogen production systems. U.S. Patent 7,146,918 B2

[9] A.R. Gizara (2007) Turbine-integrated hydrofoil. U.S. Patent 2007/0046028A1

[10] P.F. Pelz, M. Holl, M. Platzer (2016) Analytical method towards and optimal energetic and commercial wind-energy converter. Energy, Vol. 94, pp. 344-351

[11] J.C. Gilloteaux, A. Babarit (2017) Preliminary design of a wind driven vessel dedicated to hydrogen production. In Proc. of the ASME 36th International Conference on Ocean, Offshore and Artic Engineering (OMAE2017), Trondheim, Norway.

[12] K. Ouchi, J. Henzie (2017) Hydrogen generation sailing ship: conceptual design and feasibility study. In Proc. of IEEE OCEANS 2017

[13]A. Babarit, G. Clodic, S. Delvoye, J-C. Gilloteaux (2020) Exploitation of the far-offshore wind energy resource by fleets of energy ships. Part I. Energy ship design and performance. Wind Energy Science, Vol. 5, pp. 839-853A. Babarit, J.C. Gilloteaux, G. Clodic, M. Duchet, A. Simoneau, M.F. Platzer (2018) Techno-economic feasilibity of far offshore hydrogen-producing wind energy converters. International Journal of Hydrogen Energy, Vol. 43(15), pp. 7266-7289

[14] M.F. Platzer and N. Sarigul-Klijn (2009) A novel approach to extract power from free-flowing water and high-altitude jet streams. In Proc. Of the ASME 2009 3rd International conference on energy sustainability, Vol. 1, San Francisco, California, USA.

[15]M.F. Platzer, N. Sarigul-Klijn, J. Young, M.A. Ashraf, J.C.S. Lai (2014) Renewable hydrogen production using sailing ships. ASME Journal of Energy Resources Technology, Vol. 136

[16]R. Abd-Jamil, A. Chaigneau, J-C. Gilloteaux, P. Lelong, A. Babarit (2019) Comparison of the capacity factor of stationary wind turbines and weather-routed energy ships in the far-offshore. Journal of Physics: conference series, Vol. 1356

[17]ITTC: General guidelines for uncertainty analysis in resistance tests. ITTC – Recommended procedures 7.5-02-02-02, 2014

[18]https://www.wattandsea.com/fr/produits/hydro-cruising/hydro-cruising-600

[19]C.A. Marchaj (2010) Sail performance: techniques to maximise sail power. Adlard coles nautical, London, UK.

[20]G. Delhommeau, J-J. Maisonneuve (1987) Extensions du code de calcul de résistance de vagues REVA: prise en compte des effets de fond et de portance. Compte rendu des 1ères journées de l'hydrodynamique, Nantes, 1987

[21] https://en.wikipedia.org/wiki/Mirabella_V

[22]K. Siddappaji and M. Turner (2015) Revolutionary Geometries of Mobile Hydrokinetic Turbines for Wind Energy Applications. ASME International Gas Turbine Congress, Montreal, Canada

426 [23]M.F. Platzer and N. Sarigul-Klijn (2021) The Green Energy Ship: Renewable Energy from Wind
427 over Water. Springer Briefs in Applied Sciences and Technology, Springer 2021